FMCW Drone Detection Radar
ETF-Belgrade

I. Introduction

Drone detection has recently become a highly important and widely required endeavor. Commercial drones can be acquired cheaply, they can deliver various (including dangerous) payloads, and come fully equipped with high resolution cameras, capable of streaming a video footage over long distances. Espionage, breaches of privacy, and security threats from such readily available equipment are global and imminent.

Drone detection is a challenging task because drones are typically small targets (RCS of commercial drones is about −10 dBsm in most directions for frequencies in S and C bands, as we calculated by WIPL-D and show in Fig. 1). Reflections from them can easily be obscured by reflections from objects near their flight path, which a skilled operator could use to "mask" the drone approach.
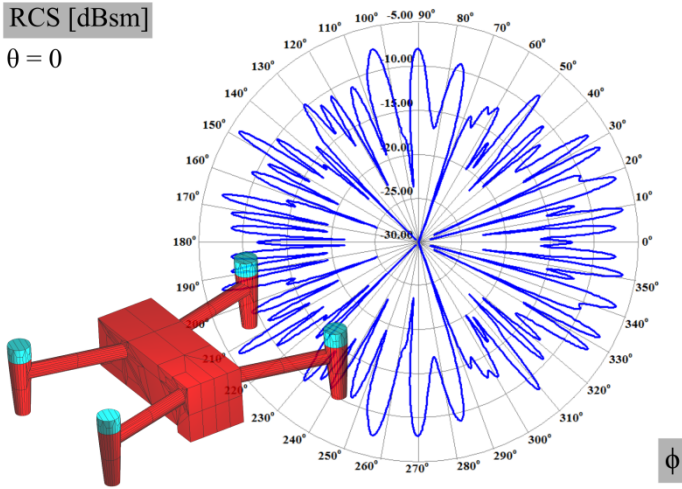

Fig. 1. A drone model in WIPL-D and its RCS at 5.8 GHz.

We have proposed a frequency modulated continuous wave (FMCW) radar which uses Doppler processing to detect moving targets and separate them from the background clutter. The proposed radar operates in the 5.8 GHz ISM band in real time. It is cheap, reliable, accurate, and simple to setup in a classroom environment.

Moreover, most of its components are fabricated as separate modules, with easily distinguishable and understandable functions, which makes the design highly suitable for educational purposes.

II. A Simplified Description of the Proposed System

Contrary to the impulse microwave radar systems, our radar is based on the FMCW principle and its block schematic is given in Fig. 2. A signal generator (ADF4158 evaluation board) emits a frequency ramp (up-chirp) carrier, as shown in blue in Fig. 3. This signal is amplified by a power amplifier (PA) and transmitted by an antenna (or antenna array) towards the target. When the reflected signal, shown in red in Fig. 3 and delayed due to traveling the distance to the target and back, is *IQ* demodulated by a copy of the transmitted signal (fed to the down-conversion blocks in Fig. 2 by a Wilkinson power divider) and filtered to remove the components at high frequencies, the resulting signal will have a spectral component at a frequency that is proportional to the delay Δt and, by extension, to the range of the target from which the reflection occurred. The *IQ* signals are sampled by analog to digital converters (ADCs) at 1 MSPS to enable subsequent digital signal processing (DSP) performed within the Xilinx Arty Z20 field programmable gate array (FPGA).
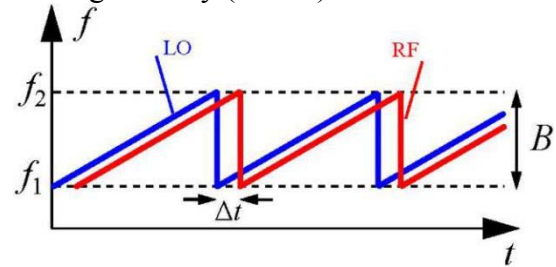

Fig. 3. FMCW detection principle.

Within the FPGA, a fast Fourier transform (FFT) is first applied to the detected signal to obtain the spectrum of the intermediate signal, which effectively contains the distribution of reflected power differentiated by the distance, i.e., range, to the target. This operation is referred to as the Range FFT. Information about the radial speed of the target is also extracted from the demodulated signal, by
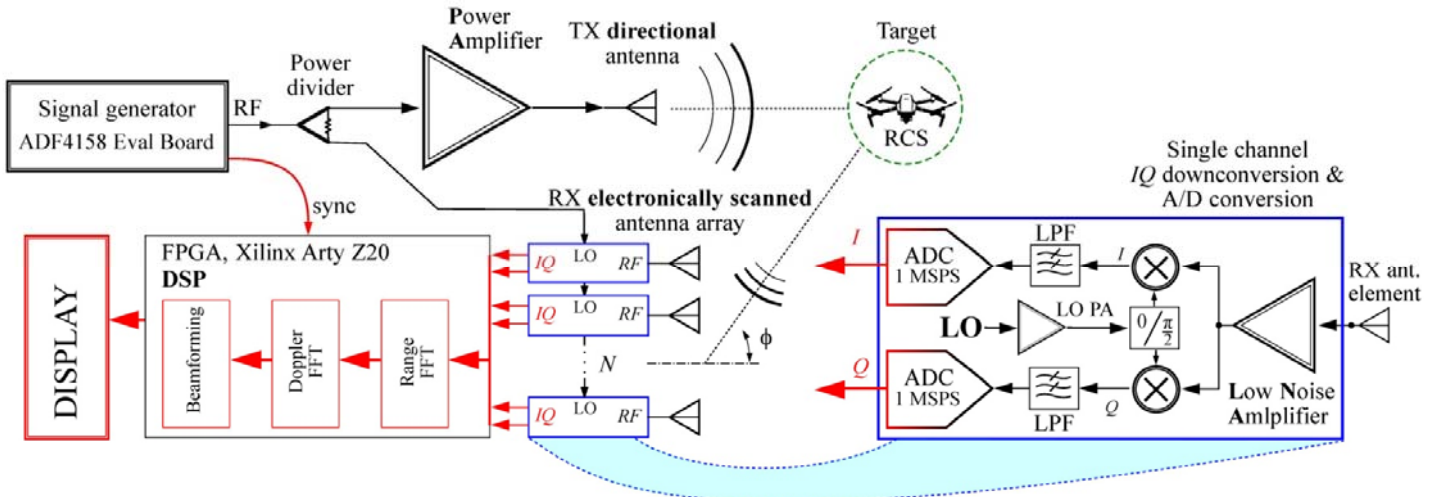

Fig. 2. A block schematic of the proposed FMCW radar drone detection system.

measuring phase differences between the reflections coming from the same range resolution cell in successive chirp intervals. The phase of reflections will change over time if the target is moving relative to the radar and the velocity of that movement can be computed from the rate of this change. This operation is called the Doppler FFT.

The Range and Doppler FFT are performed on samples from each of the receiving channels, comprising a receiving antenna element, a low noise amplifier (LNA), and a down-conversion–ADC block, separately. Multiple receiving antennas and corresponding channels are employed to obtain the azimuthal angular separation. Receiving antennas comprise a fixed, linear, uniform antenna array of printed dipoles specifically designed and matched for this purpose. The transmitting antenna is a printed antenna which illuminates the area of interest as uniformly as possible and produces a strong null in its radiation pattern towards the receiving array to minimize the Tx-Rx crosstalk.

The final output of the radar processing is the Range-Doppler (RD) map, i.e., an image displayed on a connected PC. On the simulated RD map the drone is clearly visible due to its pronounced Doppler spectrum components corresponding to the velocities other than zero, as shown in Fig. 4. in the maps obtained by simulations of the proposed radar system for various signal to noise ratios (SNRs).
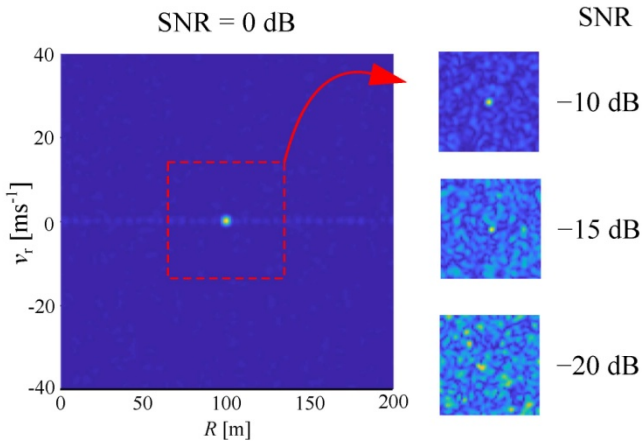

Fig. 4. Simulated RD maps for various SNRs.

We underline here that the components of the down-conversion–ADC blocks (LNAs, filters, mixers and A/D convertors), as well as the antenna array elements and transmitting arm elements (power divider, PA, and the transmitting antenna) are manufactured in-house on printed circuit boards (PCBs). On one hand, the proposed design greatly reduces manufacturing costs. On the other hand, unlike in an integrated commercial software defined radios (SDRs), all these components are clearly visible as separate modules (because they operate in the C-band). This, in turn, provides an extremely powerful and versatile educational platform, consistent with contemporary trends in FMCW radars (typically operating in mm-wave bands) available or foreseen in medical, automotive, and other industrial applications.

III. Design, Manufacturing, and Operation of Modules

In the educational spirit of this competition, a fully modular solution was the best choice. This approach facilitates easy demonstration of operation of every part of the system. Thus, most of the radar hardware components were carefully thought out, designed, and manufactured. Afterwards, the assembled components and modules were tested to see if they perform as designed. The full list of the modules is given in Table I.

Table I. The list of radar modules.

Description	Comment/Usage	Fabrication status
ADF4158 Evaluation board	Signal generator	Purchased and programmed
Mini-Circuits ZX60-83LN-S+ amplifier	Power amplifier	Purchased
Local oscillator amplifier based on the GRF 2073 chip	LO amplification	In-house
Low Noise Amplifier and Preamplifier based on GRF 2101 chip	RF input amplifiers for all channels	In-house
Wilkinson power divider 1 to 2	LO distribution	In-house
Wilkinson power divider 1 to 8	8-channels	In-house
IQ demodulator based on HMC218B mixers	8-channels	In-house
Dipole antennas	Transmitting and receiving	In-house
ARTY Z7: APSoC Zynq-7000 FPGA evaluation board	Signal processing	Purchased and programmed
Power supply board	System power	In-house
Baseband filter, amplifiers and AD converter boards	Baseband signal conditioning	In-house
FPGA shield	Communication with AD converters	In-house
Note: "In-house" stands for "Designed and manufactured in house"		

The *ADF4158 evaluation board* is used as a signal generator. It is programmed in such a way to emit a chirp signal around 5.8 GHz, which sweeps a 150 MHz bandwidth. Its output is about −7 dBm, hence amplification is needed both for emitted power and for local oscillator driving. Hence, its output is connected to two stages of amplification: first being an in-house made *preamplifier*, and the second being a *power amplifier* (PA). The power output after this amplification is about 16 dBm.
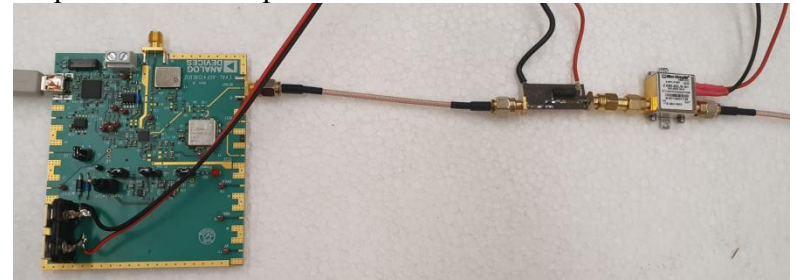

Fig. 5. ADF4158 evaluation board (left) connected to preamplifier (middle) and to PA (right).

The output from the PA is led to the one stage *Wilkinson divider*. One output from it is being emitted from the transmitting antenna, while the other is led to the 3 stage

Wilkinson divider, to be split into 8 coherent signals which are used as a local oscillator for the 8 receiving channels.
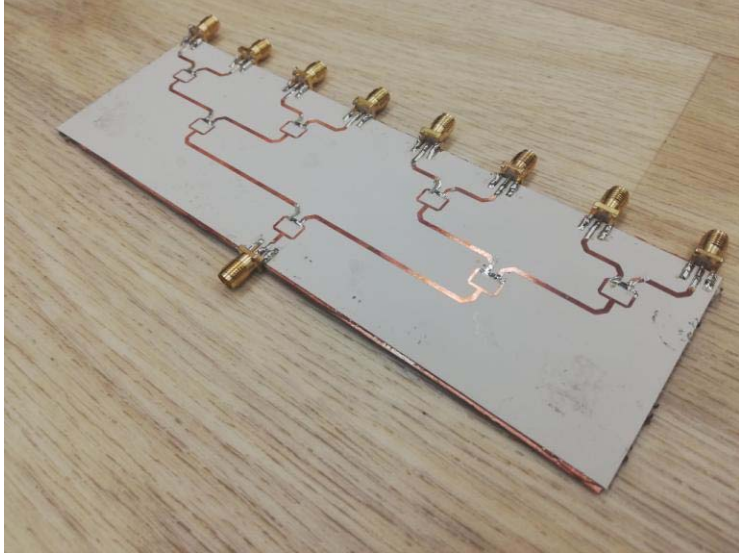

Fig. 6. 1-to-8 Wilkinson divider, used to distribute local oscillator signal to every receiver channel.

Each receiving channel consists of two boards: a *Microwave board*, printed on a high quality Rogers 3003 substrate to minimize losses, and a *Baseband board* made from a sturdy FR-4 substrate. The substrate characteristics are given in Table II.

Table II. The list of radar modules.

Substrate	ε_r	h [mm]	tanδ
Rogers 3003	3	0.51	0.0013
FR-4	4.4	1.5	0.02

The *baseband board* also serves as a mechanical reinforcement for the thin microwave board. The *microwave board*, with all of its components explained is shown in the Fig. 7:
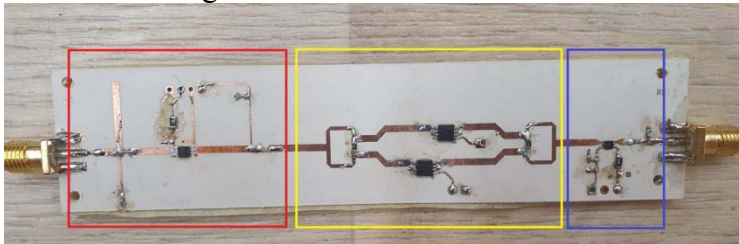

Fig. 7. Microwave board, with separate modules marked: LO amplifier (red), IQ demodulator (yellow) and preamplifier for RF signal (blue).

After splitting into 8 signals, the reference signal power drops dramatically from 13 dBm to about 3 dBm for each of the receiving channels. Each mixer requires about 13 dBm at its local oscillator port to be driven properly. Since every receiver channel contains two mixers in parallel, the local oscillator ports in all receiving channels require approximately 16 dBm. This is achieved with the *Local oscillator amplifier*, which has a 12 dB gain. Fig. 7 shows that the mixers perform well with this setup, i.e., at 1dB lower LO power.
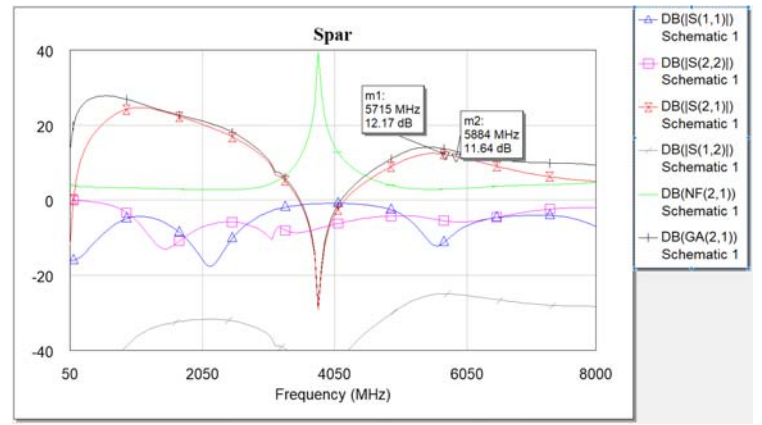

Fig. 8. S-parameters, with marked gain in 5.8 GHz band, for local oscillator amplifier.

The *Low noise amplifier* has about 11 dB gain. Its input is connected to the receiving antenna in a channel, while the output is split into two and lead into two RF ports of the mixers.

The *Antennas* are realized as printed dipole antennas, with integrated baluns and matching networks, all designed and manufactured in-house, and presented in Fig. 9.

The *IQ demodulator*, residing between the two amplifiers in each channel, consists of two HMC218B mixers and two Wilkinson dividers. The mixers are placed on a designed PCB in such a way that for one of them the local oscillator signal leads by 45° relative to the other whereas it lags by the same amount for the other.
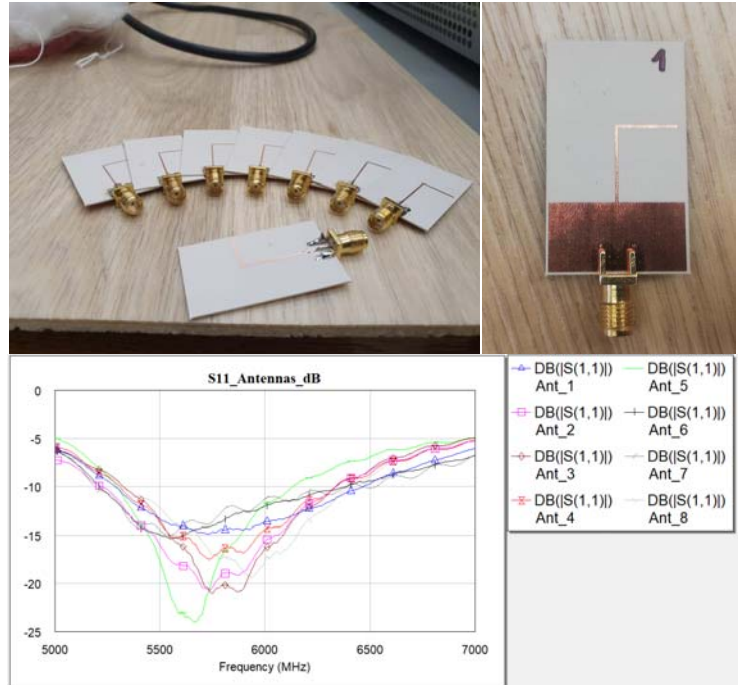

Fig. Fig. 9. Printed dipole antennas for every channel (top) and measured S11 parameters of each antenna (bottom).

This produces a 90° phase difference between two parallel mixers, which enables *IQ* demodulation. Both *I* and *Q* outputs from their respective mixers are then connected to the baseband board, which is shown on figure 10.
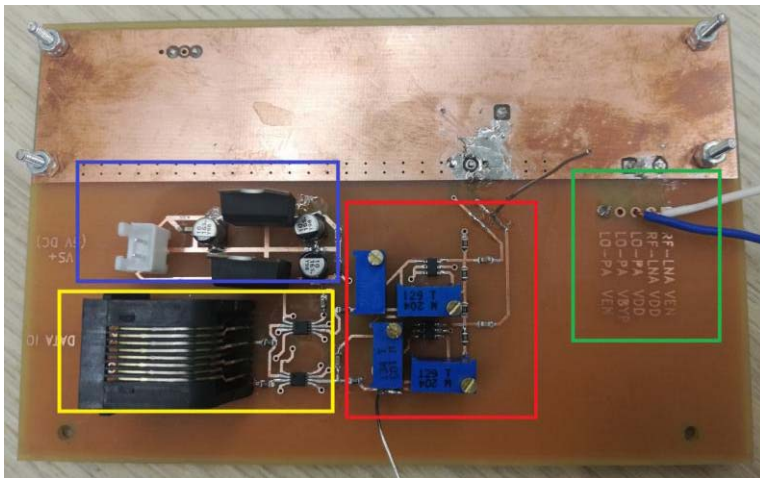
Fig. 10. Baseband board, with all of its modules: amplifier and filter (red), AD converters and digital connector (yellow), power supply for baseband (blue) and microwave components (green).

Both *I* and *Q* branches are symmetrical, so only one will be described next. IF pin from the mixer is connected to the *High pass filter*, in the form of an RC circuit, which attenuates demodulated signals up to 1 kHz. This filter helps weaken the signals originating from reflections from close objects, which are usually strong enough to saturate the baseband amplifier and/or the AD converter. The output of the filter is led to the *Baseband amplifier*. This amplifier is tunable, allowing for corrections of signal levels in case there is a slight disbalance in the output levels of mixers. The amplifier is tuned so that the full dynamic range of the AD converter is used as efficiently as possible.
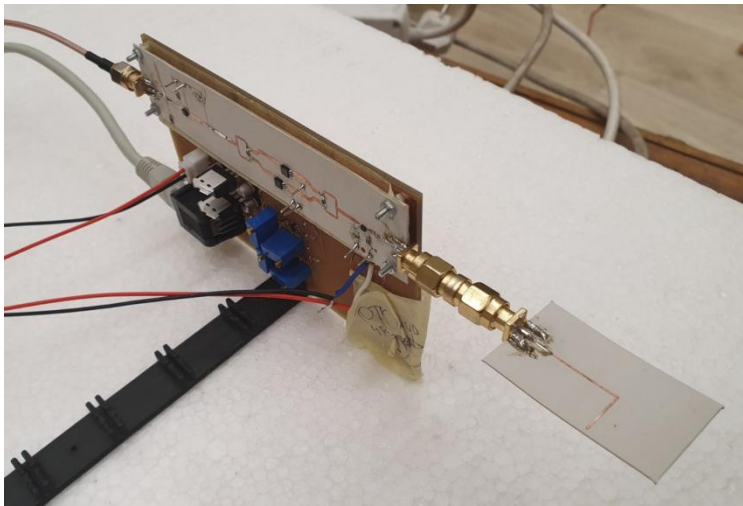

Fig. 11. Full receiver channel, with antenna and microwave board connected to the baseband board. Cable that provides LO signal and connection with FPGA can be seen in the back.

The AD converters are next connected both to the amplifiers outputs and to the FPGA over the specially designed shield. Communication between the shield and AD converters is established over UTP cables with RJ-45 connectors. Communication between FPGA board and AD converters uses the 3 wire SPI compatible interface.
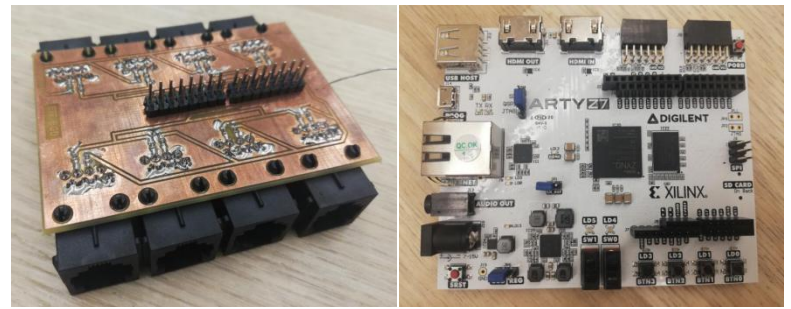

Fig. 12. Shield for FPGA board, which connects 8 receiver channels to it (left) and FPGA board itself, on which entire digital processing is done (right).

Each UTP cable is used to communicate with two AD converters from the same receiver channel. All AD converters use the same clock from the FPGA. Sampling is initiated by the trigger signal which is received from the ADF4158 board. After sampling, the entire digital signal processing is done on the FPGA.

Signal processing is achieved exactly as proposed and described in Section II of this report. An in-house stand alone application to present the results of the DSP is also developed. It presents RD maps from one of the channels, or distribution of moving reflections from all channels combined in the Range-Azimuth domain (once the beam forming algorithm is fully active with the full number of antennas).
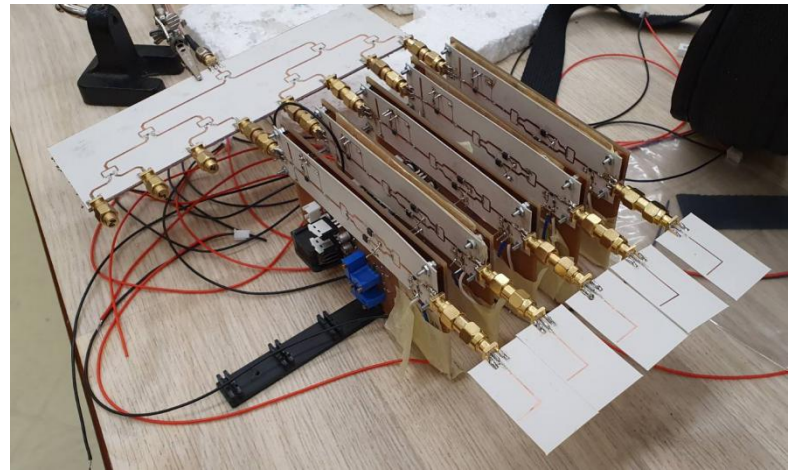

Fig. 13. Partially assembled radar with 5 receiver channels mounted on a 3-D printed carrier board.

IV Radar Experiments and Results

A multitude of problems arose due to the measures exerted as a consequence of the COVID-19 pandemic. The team faced extremely hard conditions which included a long-term lockdown and massive delays in shipping and PCB manufacturing.
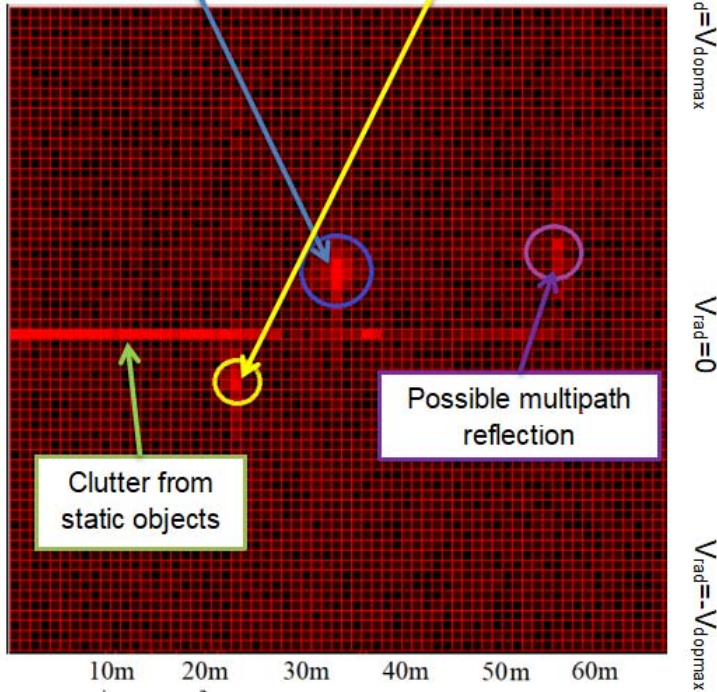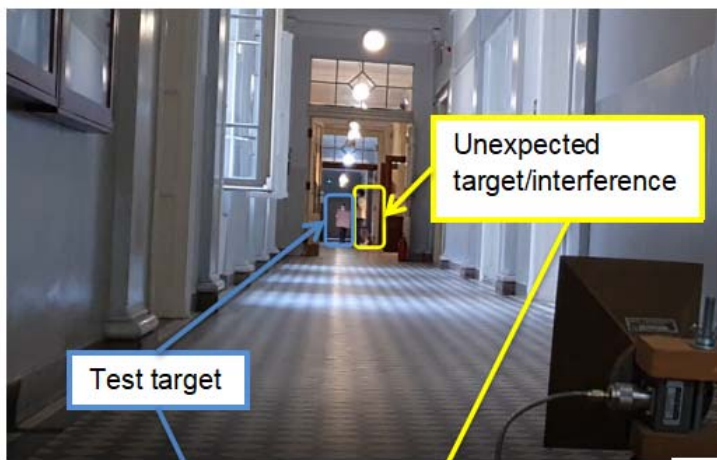
Fig. 14. Test 1 in the hallway. Scenario (top) and the RD map detected by the radar (bottom).

detected around the same range as the unexpected passer by, which might be due to crosstalk from nearby channels and/or other electronic devices.

The second test was done in the same hallway with two test targets moving at approximately the same speeds, with one moving towards the radar while the other one moving away from it. The results of this test are shown in Fig. 15. The test clearly shows the ability of radar to discern multiple close targets that are in the same resolution cell based on their different radial speeds. This multiple target detection can possibly be used in other applications, such as person detection and tracking ground radars, installed around high security objects.

Unfortunately, since the proposed design is highly dependent on the in-house hardware manufacturing and assembly, this resulted in our failure to fully integrate the designed antennas and the beamformer on time. However, we here present the results of the tests of the radar performance in real world scenarios that were carried out using the assembled modules and substitute elements (e.g., horn antennas that we had on site etc.)

The first test, carried out in our lab hallway, is shown in Fig. 14. It consists of a test target moving towards the radar. Several unexpected people walked through the zone of coverage during this test. A directional transmit antenna (lower right) is used for the purpose of this test, to mitigate reflections from the walls. The test clearly shows the capability of the radar to discern moving targets far away from the transmitter. Additionally, it shows quick real-time responsiveness, i.e., the ability to detect and show targets residing in its zone of coverage for only a few seconds. Some mild interference was
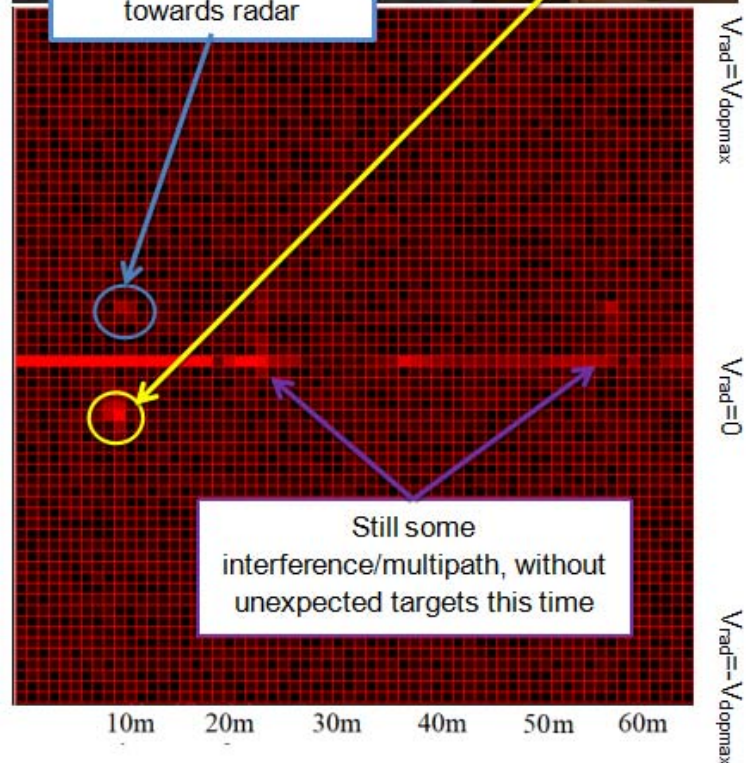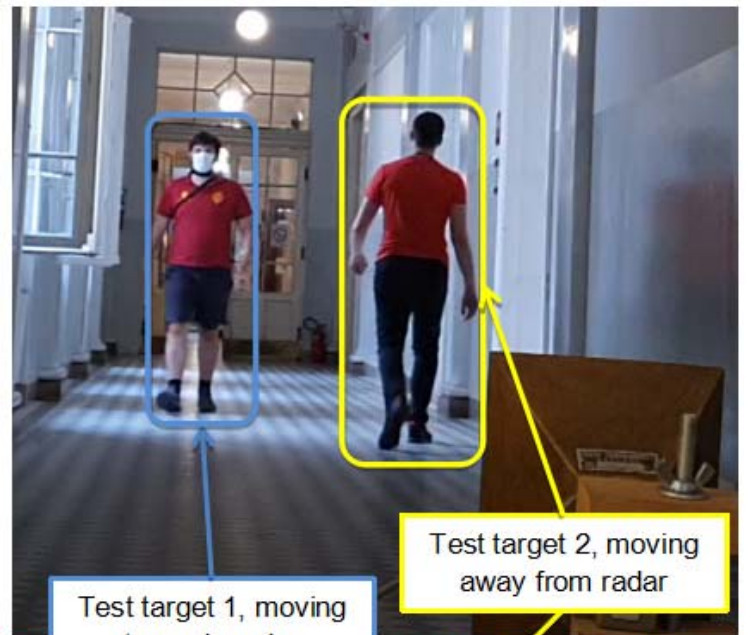

Fig. 15. Test 2 in hallway. Scenario is shown top, while the RD map detected by radar is shown on the bottom.